

Estimating Satellite Navigation Broadcast Ephemeris via Inter-Satellite and Ground-to-Satellite Ranging [†]

Andrea Testa ¹, Grzegorz Michalak ¹ , Manuele Dassié ^{1,2,*} , Karl Hans Neumayer ³ and Gabriele Giorgi ¹ 

¹ German Aerospace Center (DLR), Münchener Strasse 20, 82234 Wessling, Germany; gabriele.giorgi@dlr.de (G.G.)

² Faculty VI Planning Building Environment, Technische Universität Berlin (TUB), Strasse des 17. Juni 135, 10623 Berlin, Germany

³ German Research Centre for Geosciences (GFZ), Telegrafenberg, 14473 Potsdam, Germany

* Correspondence: manuele.dassie@dlr.de; Tel.: +49-8153-28-4963

[†] Presented at the European Navigation Conference 2023, Noordwijk, The Netherlands, 31 May–2 June 2023.

Abstract: This paper investigates the potential of performing orbit determination directly in the Earth-fixed frame based on Inter-Satellite Ranging (ISR) measurements as primary observables, combined with Ground-to-Satellite Ranging (GSR) measurements from a small regional ground network. Current Global Navigation Satellite Systems (GNSSs) use L-band pseudo-range and carrier phase measurements from global or regional ground station networks to perform dynamic Orbit Determination and Time Synchronization (ODTS), whereas sparse Satellite Laser Ranging measurements are mainly used for validation. Future GNSSs may be equipped with inter-satellite links (ISLs) to enable inter-satellite clock offset estimation, ranging and data relay. These capabilities carry the potential to significantly improve ODTS procedures. In this work, we assume a fully connected constellation via pair-wise ISLs, with measurement topology assigned by appropriate link schedulers. The satellite orbits are parametrized with the standard 15 Galileo broadcast perturbed Keplerian elements, estimated by using ISR and GSR measurements. This processing strategy eliminates the complex modeling of gravitational and non-gravitational forces, making it particularly suitable for on-board applications and offering an alternative to classical GNSS orbit determination processing architectures. The proposed orbit determination scheme can be used in case of a ground segment failure as a back-up procedure to estimate the orbits of the GNSS satellites onboard of each satellite and guaranteeing a continuous navigation message generation for the system users. The performance of the proposed method depends on a number of factors, such as the length of the data fitting interval, the measurement quality (precision and accuracy), the scheduling and geometry of ISR and GSR measurements, the number and distribution of ground stations, and the accuracy of the ground station coordinates. Preliminary results show that an orbit-only Signal-in-Space Range Error (SiSRE) in the order of 7–9 cm can be obtained by processing 2 to 3 h data with a limited set of supporting ground stations. In this study, the orbit determination scheme proposed is tested on different scenarios, providing a first assessment of attainable performance.

Keywords: on-board orbit determination, inter-satellite links, laser ranging, ground-to-satellite ranging, perturbed Keplerian elements, signal-in-space range error



Citation: Testa, A.; Michalak, G.; Dassié, M.; Neumayer, K.H.; Giorgi, G. Estimating Satellite Navigation Broadcast Ephemeris via Inter-Satellite and Ground-to-Satellite Ranging. *Eng. Proc.* **2023**, *54*, 15. <https://doi.org/10.3390/ENC2023-15463>

Academic Editors: Tom Willems and Okko Bleeker

Published: 29 October 2023



Copyright: © 2023 by the authors. Licensee MDPI, Basel, Switzerland. This article is an open access article distributed under the terms and conditions of the Creative Commons Attribution (CC BY) license (<https://creativecommons.org/licenses/by/4.0/>).

1. Introduction

Global Navigation Satellite Systems (GNSSs) transmit satellite positions and clock offsets in a navigation message that enables real-time navigation on Earth and in space. In order to generate the message, a dynamic precise orbit determination and time synchronization (ODTS) is performed, mainly based on L-band observables—pseudoranges and carrier phases—collected by ground sensor stations deployed globally (in the case of Galileo and GPS) or regionally (Beidou and GLONASS). The ODTS process estimates a large number

of nuisance parameters necessary for accurate modeling of satellite dynamics (e.g., solar radiation pressure), observation biases (e.g., antenna offsets), atmospheric delays, satellite and station clock offsets, and Earth rotation parameters for the transformation of orbits from inertial to an Earth-fixed frame [1]. This entails a computationally extensive processing of long data batches performed by the GNSS ground segment. Once the orbit determination is completed, orbital arcs are predicted, parametrized with a set of broadcast parameters, and encoded into the navigation message, which is then uploaded to the satellites. The accuracy of the broadcast ephemeris is currently at the level of decimeters to meters [1].

Optical Inter-Satellite Links (OISLs) are being considered in GNSS to provide inter-satellite ranging (ISR) and time-transfer capabilities [2–4]. By exploiting active ISR, capable of cm-level accuracy, classical Precise Orbit Determination (POD) can be significantly enhanced. It is shown in [5] that orbits can be estimated with sub-cm accuracy, with an improvement of one order of magnitude with respect to the capabilities of current GNSSs. It is of interest to investigate the potential of performing autonomous orbit determination using ISR as a primary observable, without exploitation of an extended network of ground sensor stations logging navigation data for subsequent processing.

Direct estimation of the satellite Cartesian coordinates in an Earth-fixed frame with only ISR measurements would not be feasible in general due to rank deficiency of the system and rotational and translational ambiguities. Any orbit solution solely based on ISR would be ambiguous by a rotation and a translation of the entire constellation. This can be resolved by including Ground-to-Satellite Ranging (GSR) observations from ground reference stations, by parametrizing the orbit via a reduced number of parameters (here, we used the 15 Galileo F/NAV broadcast ephemeris, i.e., the classical six Keplerian elements complemented by nine correction parameters) and by batch-processing data collected over longer time intervals. The GSR measurements can be passive, e.g., Satellite Laser Ranging, or active, e.g., optical satellite-to-ground links.

2. Functional and Stochastic Models for the Ranging Observations

For the purpose of this study, let us consider the following variables. The three-element vector $\mathbf{r}_i(t) = (x_i(t), y_i(t), z_i(t))^T$ denotes the 3D coordinates identifying the position of object i (satellite's center of mass, or ground station reference point) at time t in the Earth-Centered Earth-Fixed (ECEF) reference frame. The ranging observable, denoted with $\rho_{ij}(t)$, is the measured range between objects i and j at time t ,

$$\rho_{ij}(t) = \|\mathbf{r}_i(t) - \mathbf{r}_j(t - \Delta_{ij})\| + \varepsilon_{ij}(t), \quad \varepsilon_{ij}(t) \sim \mathcal{N}(b_{ij}(t), \sigma_{ij}^2), \quad (1)$$

where Δ_{ij} is the signal flight time and $\varepsilon_{ij}(t)$ is the measurement error (σ_{ij}^2 denotes the measurement variance, and $b_{ij}(t)$ is the measurement bias, generally time dependent). The latter is associated to a number of unmodeled effects: range biases due to residual clock offsets (we are here assuming one-way ranging based on the assumption of synchronized clocks at the two objects i and j), uncorrected relativistic effects, hardware delay calibration errors, satellite attitude modeling errors, as well as ground station coordinates uncertainties in GSR measurements. Functional Model (1) links the ranging observables with the unknown satellite coordinates. As a purely kinematic solution relying only on ISR and sparse GSR measurements is not feasible, satellite orbit is parametrized by a set of 15 parameters of a Galileo standard F/NAV navigation message [6]. We then denote the vector of unknown orbital parameters \mathbf{p} at time t_{oe} (time of ephemeris) for unknown m satellites as

$$\mathbf{p}(t_{oe}) \equiv [\mathbf{p}_1^T(t_{oe}), \mathbf{p}_2^T(t_{oe}), \dots, \mathbf{p}_m^T(t_{oe})]^T, \quad (2)$$

where $\mathbf{p}_s(t_{oe})$ is a 15-element vector containing the perturbed Keplerian parameters given in Table 1 (a), referred to satellite s at time of ephemeris t_{oe} .

Satellite Cartesian ECEF coordinates $\mathbf{r}(t)$ are computed from the 15 F/NAV orbital parameters following the user algorithm (non-linear functions) summarized in Table 1 (b) [6]. The advantage of using an orbit model based on the 15 perturbed Keplerian parameters

lies in its simplicity, which removes the need for a complex modeling of all forces acting on the satellite and their integration over time. Moreover, the data relay capabilities of the ISLs enable distributing ISR and GSR measurements across the whole constellation, potentially enabling autonomous orbit determination onboard each satellite. In this approach, the performance of orbit determination is determined by the accuracy of (a) the ranging observables, (b) the quality of the parametric model used to represent the actual satellite orbit and (c) on the length of the fitting interval (the longer the interval, the larger the errors, as it is shown in Section 5.1). It should be noted that such parametrized orbit has a very limited validity when extrapolating outside the fitting interval.

Table 1. The 15 F/NAV orbital parameters and the user algorithm.

(a) Ephemeris data definition.	
Parameter Description	
M_0	Mean anomaly
Δn	Mean motion correction
e	Eccentricity
\sqrt{a}	Square root of semi-major axis
Ω_0	Longitude of ascending node
$\dot{\Omega}$	Rate of change in longitude of ascending node
i_0	Inclination angle
\dot{i}	Rate of change in inclination angle
ω	Argument of perigee
C_{uc}	Amplitude of cosine correction to the argument of latitude
C_{us}	Amplitude of sine correction to the argument of latitude
C_{rc}	Amplitude of cosine correction to the orbit radius
C_{rs}	Amplitude of sine correction to the orbit radius
C_{ic}	Amplitude of cosine correction to the inclination
C_{is}	Amplitude of sine correction to the inclination
(b) The user algorithm.	
Computation	
$a = (\sqrt{a})^2$	
$n = \sqrt{\frac{\mu}{a^3}} + \Delta n$	
$\Delta t = t - t_{0e}$	
$M = M_0 + n\Delta t$	
$M = E - e \sin E$	
$\sin v = \frac{\sqrt{1 - e^2} \sin E}{1 - e \cos E}$	
$\cos v = \frac{\cos E - e}{1 - e \cos E}$	
$\phi = v + \omega$	
$\Omega = \Omega_0 + (\dot{\Omega} - \omega_E) \Delta t - \omega_E t_{0e}$	
$u = \phi + C_{us} \sin(2\phi) + C_{uc} \cos(2\phi)$	
$r_s = a \cdot (1 - e \cos E) + C_{rs} \sin(2\phi) + C_{rc} \cos(2\phi)$	
$i = i_0 + \dot{i} \cdot \Delta t + C_{is} \sin(2\phi) + C_{ic} \cos(2\phi)$	
$\begin{cases} x_s = r_s \cos u \cos \Omega - r_s \sin u \cos i \sin \Omega \\ y_s = r_s \cos u \sin \Omega + r_s \sin u \cos i \cos \Omega \\ z_s = r_s \sin u \sin i \end{cases}$	
$\mu = 3.986004418 \times 10^{14} \text{ m}^3/\text{s}^2$	
$\omega_E = 7.2921151467 \times 10^{-5} \text{ rad/s}$	
$c = 299792458 \text{ m/s}$	

3. Nonlinear Estimation of the Perturbed Keplerian Parameters

Let us consider a scenario in which m satellites in MEO are all equipped with two terminals for ISLs. The constellation is maintained fully connected via a link scheduling that accounts for the satellite positions, orientations and terminal field of regards; see details

in [7,8]. Moreover, GSR measurements are obtained from n ground stations. We assume that each ground station provides GSR observables to just one MEO satellite at a time, and that every satellite is only observed by one ground station at a time.

In closed-loop link topology, all satellites are assumed linked in a ‘closed-ring’ manner, with $(m + n)$ range observations (ISR and GSR) available at each epoch, and $15m$ unknowns. The ephemeris state vector \mathbf{p} can be solved by using a non-linear least squares adjustment to minimize objective function

$$\sum_{k=1}^K \left\{ (\mathbf{y}_{t_k} - \mathbf{f}_{t_k}(\mathbf{p}(t_{oe})))^T \mathbf{Q}_{\mathbf{y}_{t_k}}^{-1} (\mathbf{y}_{t_k} - \mathbf{f}_{t_k}(\mathbf{p}(t_{oe}))) \right\}, \quad (3)$$

where K is the number of epochs used, \mathbf{y}_{t_k} is the vector containing the $(m + n)$ observed ranges at time t_k , $\mathbf{f}_{t_k}(\mathbf{p}(t_{oe}))$ is the vector of nonlinear functions mapping the $15m$ broadcast parameters to the range at time t_k (given in Table 2b), and $\mathbf{Q}_{\mathbf{y}_{t_k}}^{-1}$ is the inverse of the covariance matrix of the observables.

The minimization problem in (3) is linearized by taking $\mathbf{f}(\mathbf{p}(t_{oe}))$ at each epoch t_k about an orbital set obtained with a first guess, denoted with $\hat{\mathbf{p}}^{(0)}(t_{oe})$ such that

$$\mathbf{f}(t_k, \mathbf{p}(t_{oe})) \approx \mathbf{f}(t_k, \hat{\mathbf{p}}^{(0)}(t_{oe})) + \left. \frac{\partial \mathbf{f}(t_k, \mathbf{p})}{\partial \mathbf{p}} \right|_{\mathbf{p}=\hat{\mathbf{p}}^{(0)}(t_{oe})} \cdot (\mathbf{p}(t_{oe}) - \hat{\mathbf{p}}^{(0)}(t_{oe})), \quad (4)$$

where $\left. \frac{\partial \mathbf{f}(t_k, \mathbf{p})}{\partial \mathbf{p}} \right|_{\mathbf{p}=\hat{\mathbf{p}}^{(0)}(t_{oe})}$ is a $((m + n) \times 15m)$ matrix containing the partial derivatives of the vector function $\mathbf{f}(\cdot)$ at time t_k with respect to the 15 perturbed Keplerian orbital elements of all m satellites, computed in $\hat{\mathbf{p}}^{(0)}(t_{oe})$. Expression (3) can then be linearized and rewritten in matrix form as

$$(\Delta \boldsymbol{\rho} - \mathbf{J}_f \Delta \mathbf{p}(t_{oe}))^T \mathbf{Q}_y^{-1} (\Delta \boldsymbol{\rho} - \mathbf{J}_f \Delta \mathbf{p}(t_{oe})), \quad (5)$$

where $\mathbf{J}_f = \left[\mathbf{J}_{f,t_1}(\hat{\mathbf{p}}^{(0)}(t_{oe})), \dots, \mathbf{J}_{f,t_K}(\hat{\mathbf{p}}^{(0)}(t_{oe})) \right]^T$ is the Jacobian matrix introduced in (4), containing all $((m + n)K \times 15m)$ partial derivatives of the observations over the K epochs; $\Delta \boldsymbol{\rho}$ is the residual range error, i.e., the difference between the observed ranges and the ranges computed from initial values of the orbital parameters at the linearization point; $\Delta \mathbf{p}(t_{oe})$ is the correction to the initial state vector minimizing observation residuals; and \mathbf{Q}_y is the block-diagonal covariance matrix of all observations, with diagonal components obtained from matrices $\mathbf{Q}_{\mathbf{y}_{t_k}}$.

The vector of orbital parameters is computed iteratively, starting from the initial guess:

$$\hat{\mathbf{p}}^{(i+1)}(t_{oe}) = \hat{\mathbf{p}}^{(i)}(t_{oe}) + \Delta \hat{\mathbf{p}}^{(i)}(t_{oe}), \quad \Delta \hat{\mathbf{p}}^{(i)}(t_{oe}) = \left(\mathbf{J}_f^{(i)T} \mathbf{Q}_y^{-1} \mathbf{J}_f^{(i)} \right)^{-1} \mathbf{J}_f^{(i)} \mathbf{Q}_y^{-1} \Delta \boldsymbol{\rho}. \quad (6)$$

The iterations are stopped when the norm of the increment, $\Delta \hat{\mathbf{p}}^{(i)}(t_{oe})$, falls below a given threshold. Convergence of the iterative method to a global minimum depends, among other factors, on the choice of the initial conditions. It has been observed that convergence is achieved even with an initial orbital error of a few hundred metres.

4. Data Simulation

To test the performance of the algorithm presented in Section 3, we resorted to simulation. Realistic Medium Earth Orbits (MEOs) were simulated via the software Earth Parameter and Orbit System—Orbit Computation [9], developed and provided by the German Research Center for Geosciences. The software applies up-to-date, complex dynamical models to generate realistic trajectories of Galileo satellites. The orbits were simulated with a 30 s time step for a period of 10 days. A scheduler was implemented to generate links between satellites and ground stations using available orbital data. The ISR and GSR observations are generated every 30 s. The scheduling used to define which links occur at a given epoch is planned such that satellite-to-satellite links have a persistence of at

least 1 min, whereas the ground-to-satellite links have a persistence of at least 15 min. This implies that approximately every minute, the links between satellites change, and every 15 min, a ground station links to a different satellite. Further details about the link scheduling are provided in [7,8]. The true range measurements were generated by computing the Euclidean distance (the norm term of (1)) between two satellites and between a satellite and a ground station. Gaussian noise and biases were then added to the true ranges to create observations according to stochastic Model (1): $\sigma_{\text{ISR}} = 1$ mm and $\sigma_{\text{GSR}} = 50$ mm. To emulate systematic error components, constant biases, randomly distributed in the interval 1–10 cm, were added to both ISR and GSR observations for the entire duration of the links.

5. A Note on Orbit Fitting and Orbit Extrapolation Accuracies

Before analyzing the performance of orbit determination from ISR and GSR measurements, this section focuses first on assessing the intrinsic accuracy of the broadcast orbit fitted to simulated dynamic orbits as well as on orbit accuracy when extrapolating outside the fit interval.

5.1. Accuracy of Orbit Fitting

The set of 15 F/NAV broadcast parameters (Section 2), including six Keplerian and nine perturbation corrections, has limited ability to reproduce true dynamic orbits. The orbit error is expected to be small for a short fitting interval and increase with interval length. Figure 1a shows the average accuracy over the entire constellation for a fit interval of 10 min. The orbit error is decomposed in the radial, along-track and cross-track components. Over such short intervals, the broadcast orbit model is very accurate, with fitting errors below the mm-level.

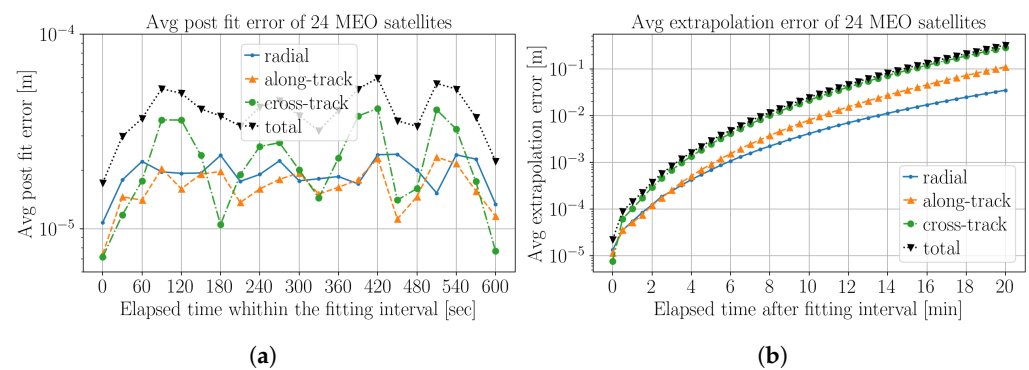


Figure 1. Average absolute post fit error and extrapolation error for the 24 MEO satellites when fitting 15 perturbed Keplerian parameters to dynamic orbits. The fitting interval is set to 10 min. (a) Post fit error. (b) Extrapolation error.

Figure 2a shows the maximum recorded Root-Mean-Square Error (RMSE) over the entire constellation for fitting intervals of 10–120 min, while Figure 2b presents results for fitting intervals of 2–6 h.

The maximum 3D (total) fitting error grows from a cm-level for two-hour intervals, a dm-level for a typical broadcast fit interval of 4 h, to an m-level when using 5 to 6 h intervals. These plots show that a cm-level accuracy is only guaranteed within 1 to 2 h fitting intervals. Therefore, any orbit determination method based on this orbit parametrization is always affected by an error equal to or larger than the orbit fitting error.

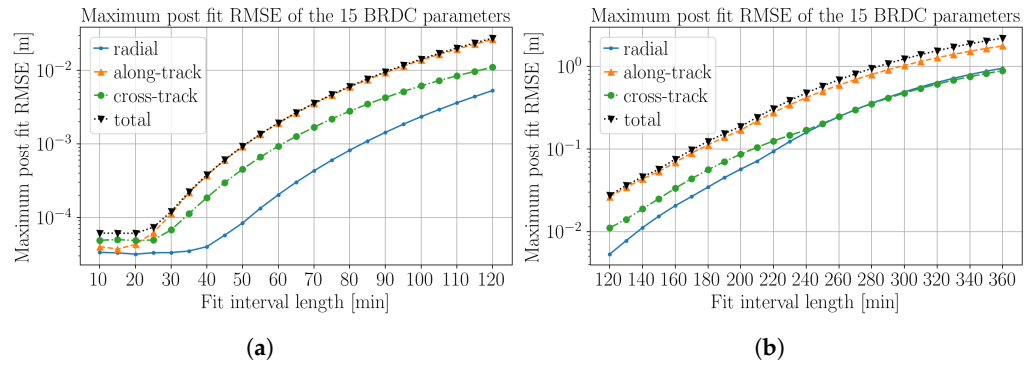


Figure 2. Maximum post fit RMSE for the 24 MEO satellites when fitting 15 perturbed Keplerian parameters to dynamic orbits, as function of the fitting interval length. (a) Fitting interval: 10 to 120 min. (b) Fitting interval: 2 to 6 h.

5.2. Accuracy of Orbit Extrapolation

The estimated broadcast parameters can be used to extrapolate satellite trajectories with the user algorithm (Table 1b) outside of the fitting interval. Figure 1b shows the average orbit extrapolation error for an interval of up to 20 min using broadcast parameters obtained from a 10 min long fit interval (cf. Figure 1a). It can be seen that the extrapolation error hits 1 cm after 8 min (elapsed time from the end of the fitting interval), and 1 decimeter after just 14 min. This rapid error growth suggests that the period of validity of the ephemeris produced when fitting to 10 min of a dynamic orbit arc should not exceed 10 to 20 min when an orbit prediction accuracy better than dm-level is targeted. This, in turn, means that in order to employ the proposed orbit determination scheme for real applications, new orbital parameters should be produced every few minutes, e.g., by implementing sliding batch processing or a Kalman filter to continuously update the estimation of the ephemeris.

6. Analysis of Orbit Determination Performance

In this section, we present simulation results of the orbit determination method detailed in Section 3 for a Galileo-like constellation of 24 MEO satellites. The 15 × 24 broadcast parameters are fitted to the ISR and GSR measurements collected over a time interval varying from 1 to 3 h. We analyze two different scenarios, with different numbers and distribution of ground stations. The first three stations, GS1–GS3 (Tromsø, Nemea and Tenerife), are located within the European geographical area. A fourth station GS4 (Papeete, French Polynesia) is added to analyze the impact of placing a station on the opposite side of the Earth.

Two scenarios are considered: (1) a regional European network of three ground stations GS1–GS3 and (2) a global network of stations GS1–GS4. Two figures of merit are used to assess the performance of the OD method. The first is the RMSE of the estimated orbit in radial, along- and cross-track directions with respect to the simulated true orbit (Section 4). The second is the orbit-only Signal-in-Space Range Error (SiSRE_{orb}), which provides a metric to express the range error introduced by the space segment. The SiSRE_{orb} combines errors in all three spatial components [10]:

$$\text{SiSRE}_{\text{orb}} = \sqrt{(W_R \Delta R)^2 + W_{AC}^2 (\Delta A^2 + \Delta C^2)}, \quad (7)$$

where ΔR , ΔA , ΔC are the average absolute radial, along- and cross-track errors, respectively, over all 24 satellites in a given time interval. Weights W_R and W_{AC} are chosen as for the Galileo system ($W_R = 0.98$ and $W_{AC}^2 = 1/61$) [10].

6.1. Noise-Free Analysis

First, in order to analyze the noise floor of the OD scheme devised, we estimated the orbital parameters from a set of error-free observations. To this aim, we set $\varepsilon_{ij}(t) = 0$ in (1) when simulating the ISR and GSR observables, and $\mathbf{Q}_y = \mathbf{I}$ in (6).

Table 2 (a) gathers the average OD RMSE and $\text{SiSRE}_{\text{orb}}$ of the 24 MEO satellites in the scenario with three European ground stations GS1-GS3. It can be observed that the longer the arcs, the larger the orbit estimation errors. The $\text{SiSRE}_{\text{orb}}$ measures less than 1.5 cm for a 1 h fit interval and grows to 9.42 cm for a 3 h fit interval.

Table 2. Average OD RMSE for 24 MEO satellites linked to a network of three or four ground stations. No noise or biases are added to the observations.

Orbital arc Length	Radial RMSE (cm)	Along-tr. RMSE (cm)	Cross-tr. RMSE (cm)	$\text{SiSRE}_{\text{orb}}$ (cm)
(a) Three Ground Stations				
1 h	1.23	2.49	3.46	1.33
2 h	2.89	19.31	23.80	4.84
3 h	7.13	35.00	39.92	9.42
(b) Four Ground Stations				
1 h	0.98	3.27	4.74	1.21
2 h	2.11	16.95	20.52	3.99
3 h	5.26	25.17	28.81	7.11

The same analysis was performed for a scenario with four ground stations, and the corresponding results are given in Table 2 (b). The addition of a fourth ground station improves the OD accuracy, mainly due to a better observation geometry, and the larger the orbital arc considered, the bigger the improvement, from 9% for 1 h intervals to 25% for 3 h intervals. It should be noted that OD accuracy is significantly lower than the accuracy of the F/NAV fit to the simulated orbits (Section 5.1) due to geometry and a much lower number of observations (ranges only).

6.2. Analysis with Measurement Errors—Regional Network

In this Section, we analyze the OD performance with simulated range measurements affected by errors and biases, as described in Section 4.

Table 3 gathers the corresponding OD RMSE and $\text{SiSRE}_{\text{orb}}$ values for arc lengths set at 1 h, 2 h and 3 h, and different combinations of simulated noise and biases. In general, for the three intervals considered, a longer observation period provides better OD results, from an m-level on 1 h arcs to a dm-level on 3 h arcs, in absence of observation biases. When adding observation biases, SiSRE increases by 40–80% with respect to a bias-free scenario, highlighting the importance of proper calibration of the terminals performing range measurements. In contrast to the analysis without noise (Section 6.1), we note that the use of a longer fitting interval has the effect of averaging the observation noise and bias, thus reducing the OD error.

Figure 3a shows the average error inside the estimated orbital arc for the 2 h scenario affected by random biases. It can be seen that the errors increase on the extremes of the fitting interval leading to a reduced accuracy of the extrapolated orbit outside the interval. This is demonstrated in Figure 3b, where total orbit extrapolation error reaches 40 m for a 1 h prediction.

Table 3. Average OD RMSE for a MEO constellation linked to a regional network of three ground stations. ISR and GSR measurements are affected by noise and biases.

Orbital arc Length	σ_{GSR} (mm)	σ_{ISR} (mm)	b_{ij} (cm)	Radial RMSE (cm)	Along-tr. RMSE (cm)	Cross-tr. RMSE (cm)	SiSRE _{orb} (cm)
1 h	50	1	None	62.83	441.24	335.83	93.98
2 h	50	1	None	7.56	44.73	45.65	11.04
3 h	50	1	None	6.32	36.46	36.23	9.04
1 h	50	1	[1, 10]	82.13	488.99	630.62	130.07
2 h	50	1	[1, 10]	12.80	90.01	75.75	19.60
3 h	50	1	[1, 10]	10.71	57.86	58.25	14.86

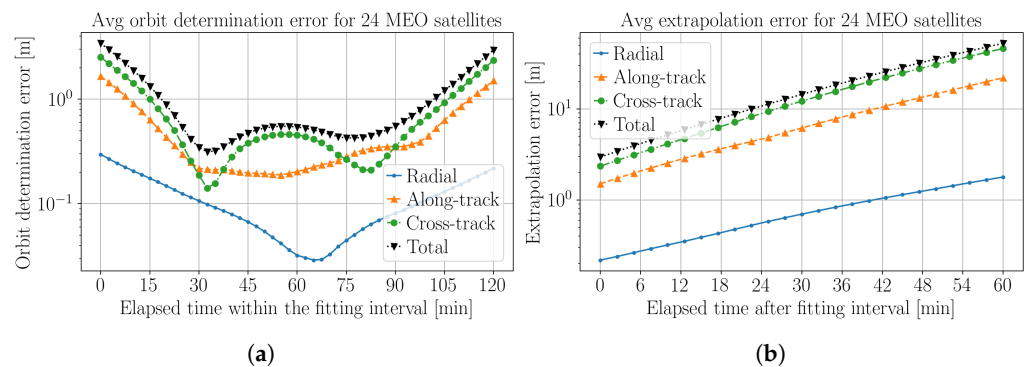


Figure 3. Average absolute post fit error and extrapolation error for the 24 MEO satellites obtained for a regional network of three ground stations, with ISR and GSR observations affected by noise and biases. The orbit parameters are estimated over a 2 h long arc. (a) Post fit error. (b) Extrapolation error.

6.3. Analysis with Measurement Errors—Global Network

When adding a fourth ground station, observation geometry improves. Orbit determination results based on this global network are shown in Table 4. It can be observed that the RMSE and the SiSRE_{orb} significantly improve by 30–45% with respect to the scenario with three ground stations, especially for shorter orbital arcs. Again, it can be seen that increasing the measurement interval reduces the negative impact of noise and biases.

The behavior of the OD error inside the estimated 2 h orbital arc is provided in Figure 4a. Similarly to the three ground station scenarios, OD errors tend to grow when approaching the extremes of the estimation interval. The average extrapolation error obtained with the parameters estimated over the 2 h fitting interval (Figure 4a) is shown in Figure 4b, where the three radial, across-track and along-track components are also provided. It can be seen that the prediction error at 1 h, approx. 25 m, is smaller than in the three regional ground station scenarios (40 m). It should be noted that the radial error is not significantly affected and remains at a 1.5 m level. Both OD and prediction performance show the benefits of including an additional ground station, located such as to significantly improve observation geometry.

Table 4. Average OD RMSE for a MEO constellation linked to a global network of four ground stations. ISR and GSR measurements are affected by noise and biases.

Orbital arc Length	σ_{GSR} (mm)	σ_{ISR} (mm)	b_{ij} (cm)	Radial RMSE (cm)	Along-tr. RMSE (cm)	Cross-tr. RMSE (cm)	SiSRE _{orb} (cm)
1 h	50	1	None	39.76	293.31	321.88	68.02
2 h	50	1	None	4.44	20.83	27.25	6.18
3 h	50	1	None	5.46	24.55	29.50	7.27
1 h	50	1	[1, 10]	49.29	334.88	457.35	87.17
2 h	50	1	[1, 10]	12.18	54.38	54.12	15.46
3 h	50	1	[1, 10]	9.78	54.47	61.64	14.24

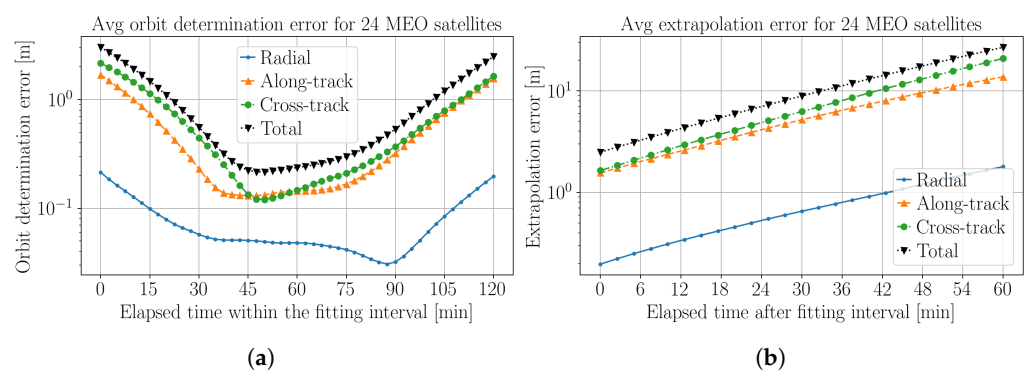


Figure 4. Average absolute post fit error and extrapolation error for the 24 MEO satellites obtained in the scenario with a global network of four ground stations, with ISR and GSR observations affected by noise and biases. The orbit parameters are estimated over a 2 h long arc. (a) Post fit error. (b) Extrapolation error.

7. Conclusions and Future Work

This work addressed the potential of performing orbit determination using inter-satellite ranging as a primary observable, without the intervention of an extended network of ground sensor stations collecting navigation data. The orbits of a GNSS MEO constellation of 24 satellites were estimated over observation intervals spanning 1, 2, or 3 h orbit arcs, aided by ground-to-satellite ranges obtained from three or four ground stations. Errors and biases were injected into the range observations to emulate realistic measurement data sets. It was shown that dm- to m-level orbit determination accuracy is attainable with a limited ground network extension. When focusing on GNSS applications, the radial orbital error component has the largest weight in defining GNSS navigation performance. To this aim, we also inspected the orbit-only signal-in-space range error SiSRE_{orb} in all the simulated scenarios, showing that SiSRE_{orb} below a decimeter can be reached when orbital arcs of sufficient length are processed, between two and three hours. However, this method cannot be further improved by extending the observed orbital arcs, since the Galileo broadcast F/NAV orbit parametrization introduces larger fitting errors.

The proposed orbit determination scheme could be used as a back-up procedure to estimate the orbits of GNSS satellites, guaranteeing a continuous navigation message generation in case of ground segment failures, as long as sparse GSR measurement can still be provided. However, we also noted a rapidly deteriorating accuracy of the predicted (extrapolated) orbit based on the estimated F/NAV parameters, which limits the validity interval of the ephemeris.

As a next step, the proposed method will be extended to process real-time observations with a Kalman filter to guarantee fast updates of the estimated orbital parameters. Additionally, in order to further improve orbit determination performance with the proposed method, it will be assessed whether low-dynamic biases affecting ISR and GSR

measurements can be co-estimated, mitigating the impact of systematic biases with an identifiable signature.

Author Contributions: Conceptualization, A.T. and G.G.; methodology, A.T. and G.G.; software, A.T., G.M., M.D. and K.H.N.; validation, A.T.; writing, A.T., G.G., G.M. and M.D.; supervision, G.G. All authors have read and agreed to the published version of the manuscript.

Funding: This research received no external funding.

Institutional Review Board Statement: Not applicable.

Informed Consent Statement: Not applicable.

Data Availability Statement: Simulated data are available for internal use only.

Conflicts of Interest: The authors declare no conflict of interest. The funders had no role in the design of the study; in the collection, analyses, or interpretation of data; in the writing of the manuscript; or in the decision to publish the results.

Abbreviations

The following abbreviations are used in this manuscript:

GNSS	Global Navigation Satellite Systems
GSR	Ground-to-Satellite Ranging
ISR	Inter-Satellite Ranging
MEO	Medium Earth Orbit
OISL	Optical Inter-Satellite Link
ODTS	Orbit Determination and Time Synchronization
POD	Precise Orbit Determination
RMSE	Root-Mean-Square Error
SiSRE	Signal-in-Space Range Error

References

1. Teunissen, P.J.G.; Montenbruck, O. (Eds.) *Springer Handbook of Global Navigation Satellite Systems*; Springer Handbooks; Springer International Publishing: Berlin/Heidelberg, Germany, 2017. [[CrossRef](#)]
2. Giorgi, G.; Schmidt, T.D.; Trainotti, C.; Mata-Calvo, R.; Fuchs, C.; Hoque, M.M.; Berdermann, J.; Furthner, J.; Günther, C.; Schuldt, T.D.; et al. Advanced technologies for satellite navigation and geodesy. *Adv. Space Res.* **2019**, *64*, 1256–1273. [[CrossRef](#)]
3. Calvo, R.M.; Poliak, J.; Surof, J.; Wolf, R. Evaluation of optical ranging and frequency transfer for the Kepler system: Preliminary laboratory tests. In Proceedings of the 2020 European Navigation Conference (ENC), Dresden, Germany, 23–24 November 2020. [[CrossRef](#)]
4. Surof, J.; Poliak, J.; Wolf, R.; Macri, L.; Calvo, R.M.; Blümel, L.; Dominguez, P.; Giorgi, G.; Agazzi, L.; Furthner, J.; et al. Validation of Kepler Time and Frequency Transfer on a Terrestrial range of 10.45 km. In Proceedings of the ION GNSS+ 2022, Denver, CO, USA, 19–23 September 2022.
5. Michalak, G.; Glaser, S.; Neumayer, K.; König, R. Precise orbit and Earth parameter determination supported by LEO satellites, inter-satellite links and synchronized clocks of a future GNSS. *Adv. Space Res.* **2021**, *68*, 4753–4782. [[CrossRef](#)]
6. Galileo–Open Service. *Signal in Space Interface Control Document (OS-SIS-ICD-V1.3)*; Technical Report; European Union: Maastricht, The Netherlands, 2016.
7. Giorgi, G.; Kroese, B.; Michalak, G. Future GNSS constellations with optical inter-satellite links. Preliminary space segment analyses. In Proceedings of the 2019 IEEE Aerospace Conference, Big Sky, MT, USA, 2–9 March 2019. [[CrossRef](#)]
8. Deprez, C.; Giorgi, G. Operational Envelope and Link Scheduling for Inter-Satellite Links in Next-Generation GNSSs. In Proceedings of the 2021 IEEE Aerospace Conference (50100), Big Sky, MT, USA, 6–13 March 2021. [[CrossRef](#)]
9. Zhu, S.; Reigber, C.; König, R. Integrated adjustment of CHAMP, GRACE, and GPS data. *J. Geod.* **2004**, *78*, 103–108. [[CrossRef](#)]
10. Montenbruck, O.; Steigenberger, P.; Hauschild, A. Broadcast versus precise ephemerides: a multi-GNSS perspective. *GPS Solut.* **2015**, *19*, 321–333. [[CrossRef](#)]

Disclaimer/Publisher’s Note: The statements, opinions and data contained in all publications are solely those of the individual author(s) and contributor(s) and not of MDPI and/or the editor(s). MDPI and/or the editor(s) disclaim responsibility for any injury to people or property resulting from any ideas, methods, instructions or products referred to in the content.